apply a Minimum Energy Flow (MEF) method which is capable of estimating both incompressible and compressible flows from time-varying density images. Both the MEF and force-estimation techniques are applied to experimentally obtained density images, spanning spatial scales from micrometers to several kilometers. Using density image sequences describing cell splitting, for example, we show that cell division is driven by gradients in apparent pressure within a cell. Using density image sequences of fish shoals, we also quantify 1) intershoal dynamics such as coalescence of fish groups over tens of kilometers, 2) fish mass flow between different parts of a large shoal, and 3) the stresses acting on large fish shoals. IEEE Transactions on Pattern Analysis and Machine Intelligence 33(6), pp. 1132-1146 (2011)



## Session 2aBA

## Biomedical Acoustics: Biomedical Ultrasound Imaging Instrumentation

Lei Sun, Cochair
*sun.lei@inet.polyu.edu.hk*

Qifa Zhou, Cochair
*qifazhou@usc.edu*

### *Invited Papers*

**9:20**

**2aBA1. High frame rate velocity-coded speckle imaging platform for coherent blood flow visualization.** Alfred C. H. Yu and Billy Y. S. Yiu (Medical Engineering Program, The University of Hong Kong, alfred.yu@hku.hk)

Non-invasive imaging of blood flow at over 100 fps (i.e. beyond video display range) is known to be of clinical interest given that such a high frame rate is essential for coherent visualization of complex hemodynamic events like flow turbulence. From a technical standpoint, getting into this frame rate range has became possible with the advent of broad-view ultrasound imaging paradigms that can track motion over an entire field-of-view using few pulse-echo firings. Leveraging on an imaging paradigm known as plane wave excitation, a novel high-frame-rate flow visualization technique has been developed to depict both blood speckle motion (using B-flow imaging principles) and flow velocities (using conventional color flow imaging principles). Experimental demonstration of this method has been carried out using a channel-domain research platform that supports real-time pre-beamformed data acquisition (SonixDAQ) and a high-throughput processing engine that is based upon graphical processing unit technology (developed in-house by the authors). In a case with a 417 fps frame rate (based on 5000 Hz pulse repetition frequency and slow-time ensemble size of 12), results show that high-frame-rate velocity-coded speckle imaging can more coherently trace fast-moving blood flow than conventional color flow imaging. Acknowledgement: Research Grants Council of Hong Kong (GRF 785811M)

**9:40**

**2aBA2. An open system for intravascular ultrasound imaging.** Weibao Qiu, Yan Chen, Wang Fai Cheng, Yanyan Yu, Fu Keung Tsang, Jiyan Dai (The Hong Kong Polytechnic University, qiu.weibao@connect.polyu.hk), Qifa Zhou (University of Southern California), and Lei Sun (The Hong Kong Polytechnic University)

Cardiovascular disease is the main causes of morbidity and mortality due to lumen stenosis and atherosclerosis. Intravascular ultrasound (IVUS) is able to delineate internal structures of vessel wall with fine spatial resolution. However, IVUS is insufficient to identify the fibrous cap thickness and tissue composition of atherosclerotic lesions, the key factors to stage atherosclerosis and determine appropriate treatment strategies. Currently, novel techniques have been developed to determine tissue composition, which require an open IVUS system to accommodate these techniques for comprehensive plaque characterization. This paper presents the development of such an IVUS system with reconfigurable hardware implementation, programmable image processing algorithms, and flexible imaging control to support an easy fusion with other techniques to improve the diagnostic capabilities for cardiovascular diseases. In addition, this IVUS utilized a miniaturized ultrasound transducer constructed by PMN-PT single crystal for better piezoelectric constant and electromechanical coupling coefficient than traditional PZT ceramics. Testing results showed that the IVUS system could offer a minimum detectable signal of 25$\mu$V, allowing a 51dB dynamic range at 47dB gain, with a frequency range from 20MHz to 80MHz. Finally, phantom imaging and in vitro vessel imaging were conducted to demonstrate the performance of the open system for IVUS applications.

# INTRODUCTION

Cardiovascular disease is one of the main causes of morbidity and mortality although increasing utilization of established preventive therapies is applied[1]. Atherosclerosis is a principal consequence of cardiovascular disease as the narrowing of the arteries, which can lead to ischemia of the heart resulting in infarction[2]. Clinically, plaque is considered the main determinants of luminal narrowing in atherosclerosis. The risk of atherosclerosis death is increased significantly by the vulnerable plaque rupture which may cause thrombus-mediated critical events such as myocardial infarction[3, 4]. There are three main factors to determine plague vulnerability: thickness of the fibrous cap, size and composition of the atheromatous lipid core, and inflammation within or adjacent to the fibrous cap[5]. The plaque is more prone to rupture with the thin fibrous cap in a high circumferential stress at the luminal border. The risk of plaque rupture also increased if a highly thrombogenic lipid-rich core is included in the plaque with a large size and a low consistent composition[5].

Angiography is a routine diagnostic technique to determine the location and degree of atherosclerotic vessel stenosis[6]. But it cannot acquire structural information of the stenotic vessel walls for accurate assessment of atherosclerotic disease burden[7]. Intravascular ultrasound (IVUS) imaging, which can assess the morphological properties of blood vessels directly by cannulating a miniature catheter into the arteries[8, 9, 10], has been increasingly used for clinical investigations, such as guiding the placement of stent[11], or evaluation of the therapy strategies and the follow-up examinations in heart transplant recipients[12, 13]. Although the IVUS has been extensively used clinically in recent years, IVUS imaging is still insufficient to visualize the thin fibrous cap thickness[14]. The reliability of IVUS is also challenging especially for characterization of plaque composition[8, 15]. Novel imaging strategies have been developed recently to investigate atherosclerosis such as near-infrared spectroscopy[16, 17], optical coherence tomography[10, 18], fluorescence spectroscopy[19], and photoacoustic imaging[20]. These techniques have intrinsic advantages and are sensitive to either plaque structure (luminal diameter, wall thickness, plaque volume, etc.) or composition. However, none of these techniques alone can provide complete information concerning various markers involved in plaque vulnerability and rupture, which may encompass both structure and composition. A system combining IVUS technique with these novel imaging modalities could achieve valuable information to improve the diagnostic accuracy[21, 22, 23]. The implementation of these new techniques requires an IVUS system to have open structures, so that it can easily accommodate other techniques to achieve comprehensive information. Such an open system should have reconfigurable hardware circuitry, programmable processing algorithms, and flexible imaging control to achieve multi-modality capability for accurate diagnosis of the cardiovascular diseases.

In this paper, we present the development of such an open IVUS imaging system that can support easy fusion of other techniques for multi-modality diagnosis of cardiovascular diseases. This system achieved reconfigurable hardware circuitry, programmable processing algorithms, flexible imaging control, and raw RF data acquisition. Field programmable gate array (FPGA) was employed as a core microprocessor to accomplish flexibility, diversity, and real-time imaging. Low noise electronics were used to support large signal-to-noise ratio (SNR) and high precision data acquisition[24, 25, 26]. Two high speed data transfer schemes, the PCI Express (PCIE) interface and the universal serial bus (USB), were implemented in this system for fast data

transmission. The system design was based on electronic components and printed circuit board (PCB) for a compact and cost-effective implementation.

The catheter probe design for IVUS applications is challenging since the size of ultrasonic transducer is extremely small and the center frequency is high. Traditionally, the PZT material is used for IVUS as its high electromechanical coupling factor and piezoelectric constant. Recently, the lead magnesium niobate-lead titanate (PMN-PT) single crystal has demonstrated superior piezoelectric properties for high frequency high performance ultrasonic transducers[27]. PMN-PT single crystal possesses higher piezoelectric constant and larger electromechanical coupling coefficient than that of conventional PZT ceramics. In this paper, a miniaturized catheter was fabricated using PMN-PT single crystal and demonstrated high sensitivity and broad bandwidth. Moreover, a small rotary motor was developed in this paper to drive the catheter probe to achieve cross-sectional view of the blood vessels.

This paper is organized as follows, in the METHODS section, the open IVUS system development, the miniaturized catheter fabrication, and construction of rotary motor are described in detail. Electronic testing, phantom and tissue imaging results are presented in the RESULTS section, followed by CONCLUSIONS.

## METHODS

The block diagram of the designed open IVUS system is shown in Fig. 1. A miniaturized ultrasonic transducer was placed at distal end of the catheter to transmit and receive ultrasound signal. A customized rotary motor was fabricated to drive the catheter to acquire a cross-sectional view of target vessels. A pulse generator generates high voltage short pulse to excite the transducer at desired frequency and spectrum specifications. An FPGA-based high speed digital receiver is developed to process the ultrasound echo signal for programmability and flexibility. The receiver incorporates the front-end electronics such as amplifier, filter, and analog-to-digital converter (ADC), FPGA microprocessor, PCIE and USB interfaces. The system is designed on electronic components and PCB for a compact implementation. A personal computer is employed for image display and data storage for further investigations. Graphical user interface software is programmed in Visual C++ and compiled in Visual Studio 2005 Professional Edition (Microsoft Corporation, Redmond, WA) to process and display the real-time IVUS images. High speed data transfer scheme can be chosen between PCIE and USB according to the specific applications.

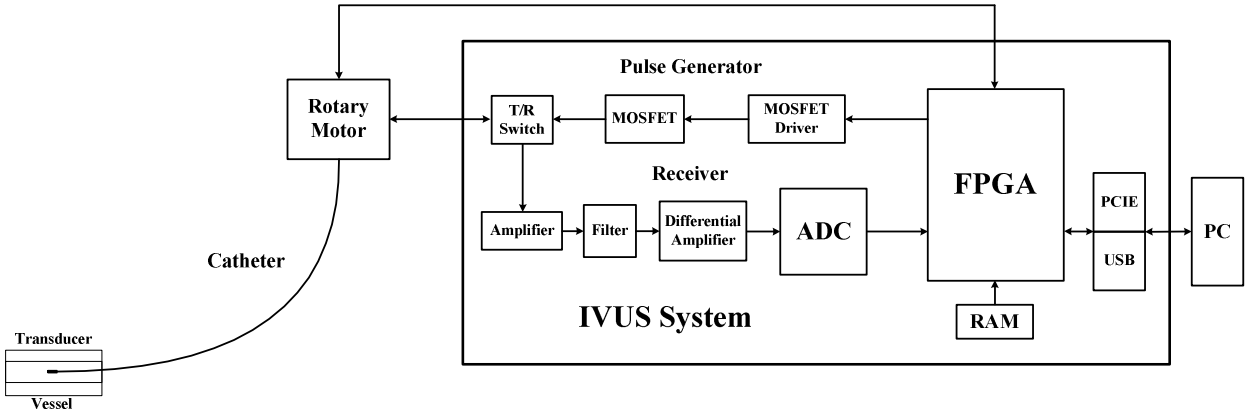


Fig. 1. The block diagram of the open system for intravascular ultrasound imaging.

### A. *Miniatruized Catheter Probe*

A 32MHz single element ultrasound transducer was fabricated using PMN-PT single crystal. The transducer was designed using the Piezo CAD simulation software (Version 3.03 for Windows, Sonic Concepts, Woodinville, WA) based on KLM model. The transducer included four components: backing material, active element, matching layer, and metal probe. As the matching layer and protecting layer, parylene C (Specialist Coating Systems, Indianapolis, IN) was evaporated onto the transducers by a parylene deposition system (model PDS 2010, Specialist Coating System). A conductive epoxy (E-solder 3022, Von Roll Isola, New Haven, CT) was casted on the single crystal as the backing material of the transducer. In addition, the transducer probe was wired with a flexible metal drive cable (Asahi Intecc co., ltd., Pathumthani, Thailand). The metal drive cable is 1.5m long and 0.7mm in diameter for the catheter.

### B. *Pulse Generator*

The designed pulse generator for this open IVUS system incorporated a bipolar pulse generation scheme. A programmable FPGA component (Cyclone III, EP3C16F484C6N, Altera Corporation, San Jose, CA) was employed to control the timing and spectrum characteristics of the high voltage short pulse. Therefore, the pulse generator can be easily adjusted to support transducers with different center frequency as well as to match with the spectrum of individual transducer to acquire the optimized performance. Two metal-oxide-semiconductor field effect transistor (MOSFET) drivers (EL7158, Intersil Corporation, Milpitas, CA) were employed to accomplish the voltage level shift and high current output to excite the high-speed MOSFET pair (TC6320, Supertex Inc., Sunnyvale, CA). The MOSFET pair could offer more than 150Vpp breakdown voltages and a 2A output peak current, which made it suitable to produce a high-voltage pulse for IVUS imaging. Finally, the pulse generator performance was evaluated by a digital oscilloscope (LeCroy wavepro 715Zi, LeCroy Corp., Chestnut Ridge, NY) with a series of attenuators (Mini-Circuits, Brooklyn, NY).

### C. *Digitial Receiver*

A low noise preamplifier (SMA231, Tyco Electronics Co., Berwyn, PA) was used as the first stage to achieve a good SNR, followed by a second stage amplifier (THS4509, Texas Instruments Inc., Dallas, TX) to achieve adequate amplification gain. A high speed, 11 bits ADC (ADS5517, Texas Instruments Inc., Dallas, TX) with a maximum sampling rate of 200 mega-samples per second (MSPS) was utilized for signal digitization. After the digitization, the signal was transferred to FPGA through low voltage differential signaling (LVDS) bus. A high performance FPGA (Stratix II EP2S60F672C5, Altera Corporation, San Jose, CA) was employed for programmable signal/image processing and high speed data transfer. It could achieve various programmable algorithms such as band-pass filter, Hilbert transform, envelop detection and digital scan conversion. A 128M bits synchronous dynamic random access memory (SDRAM) (MT48LC8M16A2, Micron Technology Inc., Boise, ID) was configured to FPGA for temporary data storage. Finally, the processed images or raw RF data were transferred to a computer through a PCIE interface component (PEX8311, PLX Technology Inc, Sunnyvale, CA) or USB interface component (CY68013A, Cypress, San Jose, CA) for displaying, storage or post-processing.

The performance of the open IVUS system electronics was tested with the following aspects. The linearity and flatness of gain in receiver was tested by a 240MHz function generator (AFG 3251, Tektronix Inc., Beaverton, OR), and a digital oscilloscope (LeCroy wavepro 715Zi, LeCroy Corp., Chestnut Ridge, NY). The noise level of the system was tested by measuring the minimum detectable signal level and dynamic range. Five-cycle sinusoidal signal generated by the function generator was attenuated by a series of attenuators and then sent to the IVUS receiver. After passing through the front-end electronics, the amplitude of the weak signal that could just be identified from the background noise determined the minimum detectable signal level. Given the input range of the high speed ADC (2Vpp), the dynamic range can be derived from the gain and the minimum detectable signal level.

As a field programmable microprocessor, the FPGA can achieve various functionalities normally realized by hardware circuitry. Moreover, the functions can easily be changed or modified by reprogramming the FPGA without change of hardware. Thus, the FPGA technology can significantly improve the system flexibility and diversity by programmable and reconfigurable algorithms. Fig. 2 shows a representative structure of image processing algorithms for real-time IVUS imaging. The entire processing algorithms could be easily reprogrammed according to different applications. A double data rate LVDS buffer is used to decode the digitized ultrasound echo data through high speed ADC. Both the rising and falling edges of clock are employed for data transferring to achieve high data throughput. A band-pass filter (BPF) is used to remove noise out of spectrum of interests. The coefficient of the BPF is reconfigurable for individual transducers with different center frequency and bandwidth. The filtered signal is then sent to the envelope detector to achieve envelope extraction. The acquired envelope data are then undergone digital scan conversion and logarithmic compression for coordination conversion and data compression, respectively. Finally, image data are sent to a personal computer through PCIE or USB interface for display and storage. A SDRAM controller is employed to buffer data with external SDRAM for flexible digital scan conversion and logarithmic compression.

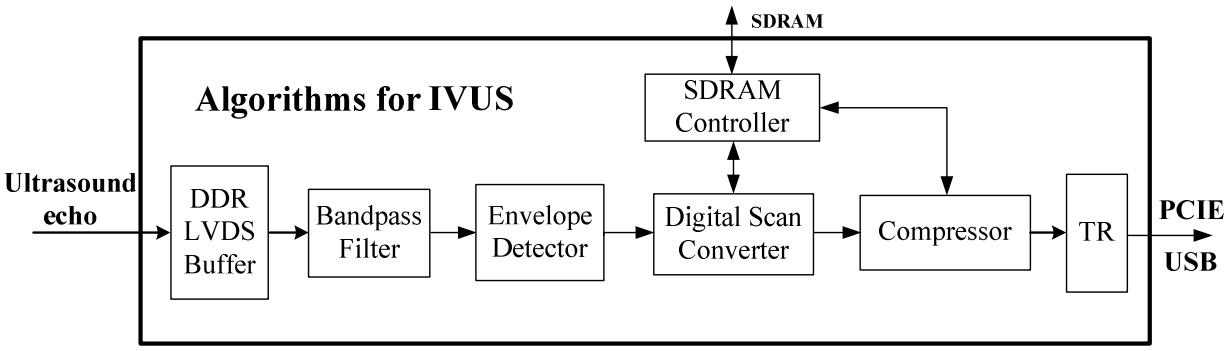


Fig.2. The algorithms implemented in FPGA for real-time IVUS imaging.

### *D. Rotary Motor*

A rotational motor is designed and implemented to acquire cross-sectional view of blood vessels through rotating the catheter. The detailed structure of the rotary motor is shown in Fig. 3.

The design used a direct current motor, which was installed in a metal box, to rotate a horizontal bevel gear. The torque transferred from the horizontal bevel gear was passed to a vertical bevel gear fixed on a hollow shaft. The hollow shaft could be rotated at certain speed driven by the gears and motor. A coaxial cable inside the hollow shaft was connected to a SMA connector to wire the catheter. The other end of the cable was connected to a slip ring (Sen Ring Electronics Co., Limited, Shenzhen, China). The slip ring is a rotary coupling device, which is used to transfer ultrasound signal between a stationary IVUS circuitry to a rotating catheter. An optical sensor was used to generate a trigger signal for system synchronization.

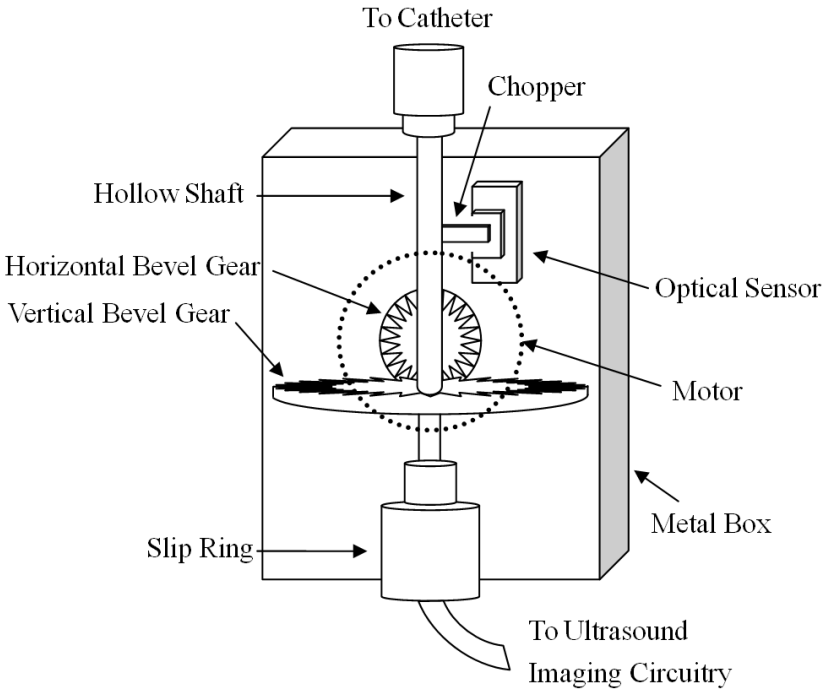


Fig. 3. The detailed structure of the rotary motor.

## IV. RESULTS

The photographs of the open IVUS system prototypes are shown in Fig. 4. Fig. 4(a) shows the entire system. The ultrasound transducer catheter and rotary motor are shown in Fig. 4(b) and Fig. 4(c), respectively. The pulse generator and digital receiver are shown in Fig. 4(d) and Fig. 4(e), respectively based on eight-layer PCB design incorporating state-of-the-art electronics.

### *A. Catheter*

The active element of the transducer in the catheter is a piece of 70μm thick PMN-PT single crystal with a size about 0.6mm × 0.6mm. Fig. 5 shows the pulse-echo waveform and frequency spectrum of the transducer measured by a Panametrics 5900PR pulser/receiver (Olympus NDT Inc., Waltham, MA) and an oscilloscope. The receiver gain of 5900PR pulser/receiver is 16dB. The measured center frequency of the catheter is about 32MHz. The -6dB bandwidth and the insertion loss of is 62.7% and of -25 dB, respectively.

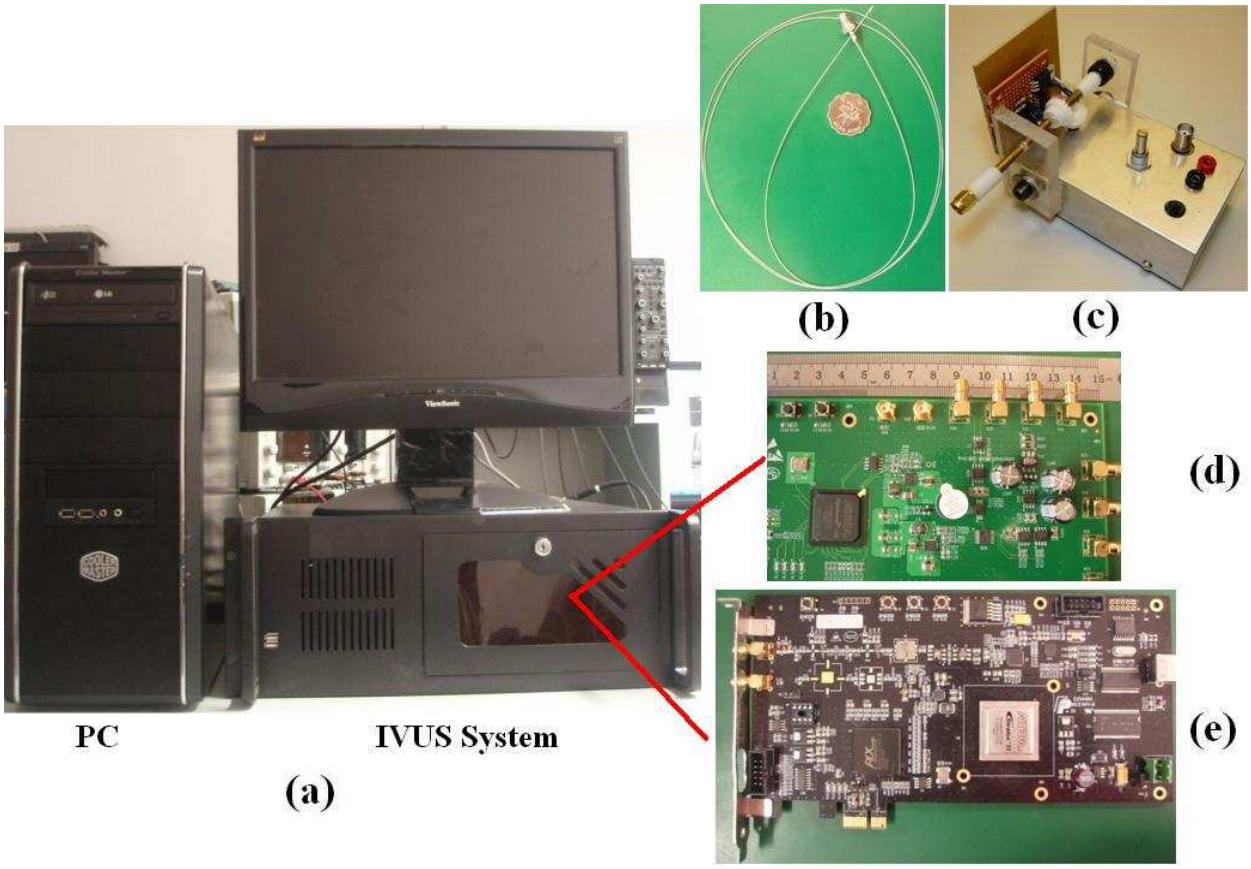


Fig.4. (a) Photopgraph of the entire open IVUS system. (b) IVUS catheter. (c) Small size rotary motor. (d) High voltage pulse generator. (e) High speed digital receiver.

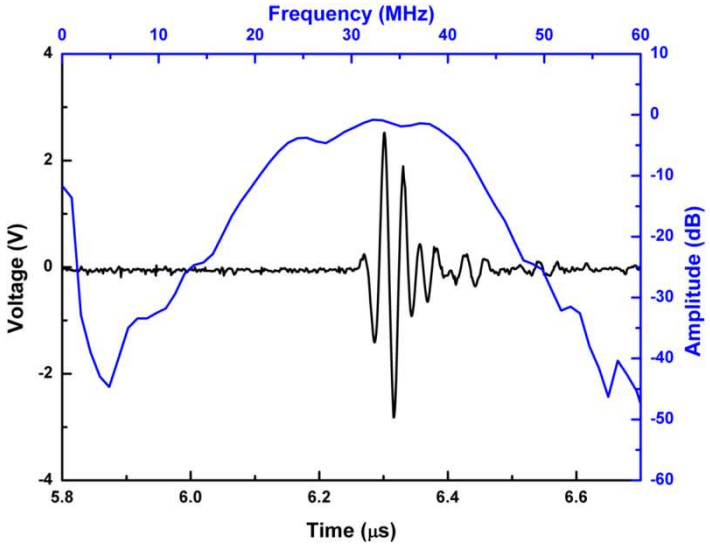


Fig. 5. The pulse-echo waveform and frequency spectrum of the IVUS catheter. (32MHz center frequency, 62.7% bandwidth, and -25 dB insertion loss).

### B. *Electronics*

TABLE 1. Electronics performance of the open system.

| **Articles** | **Performance** |
|---|---|
| Frequency range | 20-80MHz |
| High voltage tunable pulse | Up to 160V Vpp |
| Gain | 47dB |
| Gain fluctuation | ±1.2dB |
| ADC | 11bits, 200MSPS |
| Minimum detectable signal | 25μV |
| Dynamic range | 51dB |
| Software improved dynamic range | 55.8dB |
| Data transferring speed | 150MByte/s (PCIE)<br>20MByte/s (USB) |

Table 1 summarizes the performance of the IVUS system electronics. The highest amplitude of bipolar pulse was 160Vpp with adjustable center frequency and bandwidth. Table 1 also demonstrates that the maximum gain of the front-end electronics is 47dB with good linearity at a maximum fluctuation of less than ±1.2dB between 10MHz and 90MHz. The minimal detectable signal level of the system receiver is less than 25μV. Given the input range of the high speed ADC (2Vpp), the system can allow a 51dB dynamic range at 35MHz center frequency.

### C. *FPGA algorithms and processing speed*

The software-based band pass filter (BPF) was programmed in the FPGA to further remove the noise and improve the signal SNR. Quantitative analysis showed that approximately 4.8dB SNR improvement was achieved after applying the BPF, which increased the system dynamic range to 56dB.

TABLE 2. Resource utilizations of FPGA.

| **Articles** | **Resource utilization** |
|---|---|
| Adaptive look-up tables (ALUTs) | 4855 (10%) |
| Pins | 216(44%) |
| DSP block 9-bit elements | 64 (22%) |
| Memory bits | 53152 (2%) |
| PLLs | 2 (33%) |

Table 2 lists FPGA resource utilization in the FPGA for only IVUS imaging. There are significant amount of resources left to support the combination of other techniques with IVUS for comprehensive analysis of cardiovascular disease.

The algorithmic scheme implemented in the FPGA can achieve high speed imaging by pipe-line signal processing. The data transferring speed was higher than 150MByte/s and 20MByte/s for PCIE or USB interface respectively. At the image size of 512×512 pixels, the system can process a maximum of 572 or 76 images per second for PCIE and USB, respectively. Current frame rate is limited by the rotary motor speed, and it can be significantly improved if a faster rotary motor is used. With the current utilization of FPGA resources, much more

complicated signal processing may be implemented to acquire useful information than vessel morphology, e.g. virtual histology (tissue characterization based on ultrasound raw RF data).

### *D. Imaging Experiments*

The image quality of the IVUS system was evaluated first by a customized tungsten wire phantom. The wire phantom consisted of four 20μm diameter tungsten wires (California Fine Wire Co., CA) located at different depths. The ultrasound image of this wire phantom is shown in Fig. 6(a) with a dynamic range of 48dB without noticeable noise.

A tissue mimicking phantom was fabricated and imaged as shown in Fig. 6(b). The phantom fabrication procedure followed Madsen's method[28]. In short, it consisted of a mixture of deionized water, high-grade agarose, preservative, propylene glycol, filtered bovine milk, and glass-bead. The phantom could generate tissue mimicking attenuation and backscattering at high frequency range. The experiment shows that the penetration depth of this IVUS system is more than 4mm, which is adequate for most IVUS applications.

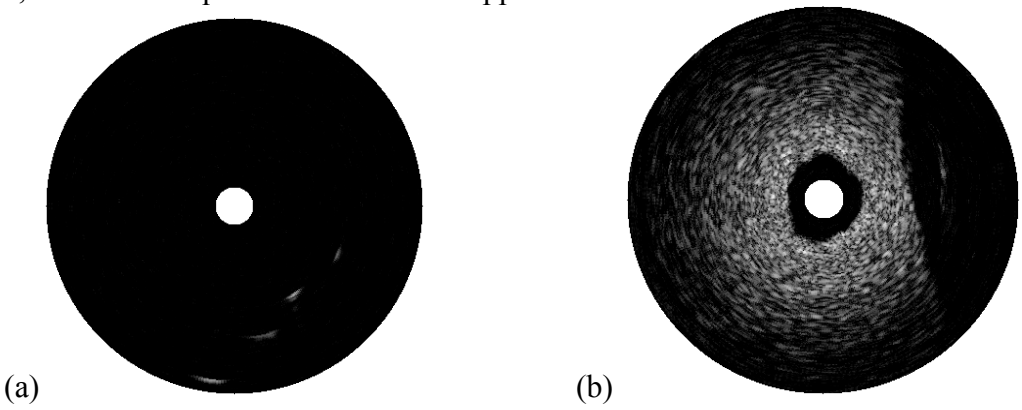

(a) (b)

Fig. 6. Phantom evaluation of the designed IVUS system. (a) Tungsten wire phantom image. (b) Image of tissue mimicking phantom.

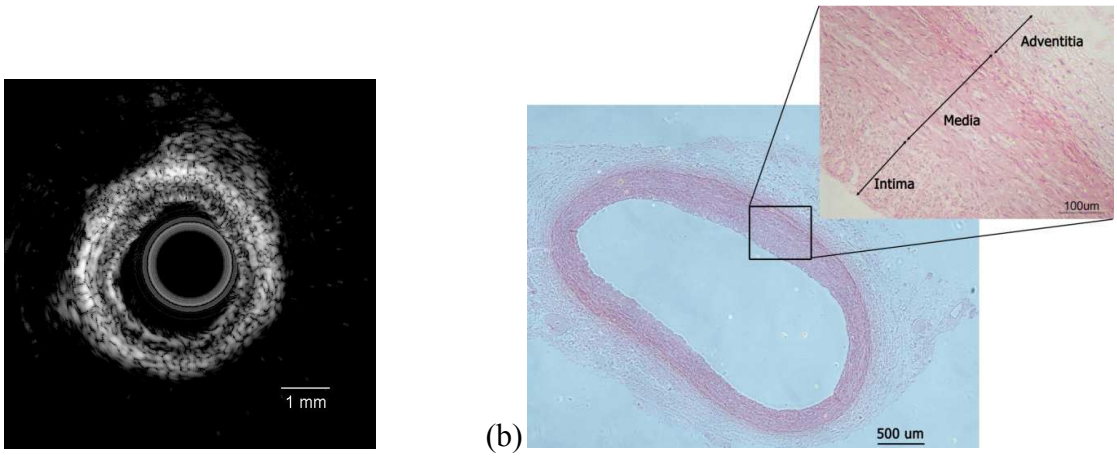


(a) (b)

Fig.7. *In vitro* imaging of swine coronary artery by IVUS and histology. (a) Ultrasound image. (b) Histological section.

The ultrasound image of *in vitro* swine coronary artery fixed in a water tank is shown in Fig. 7(a). In the ultrasound image, different layers of the artery can be clearly identified. The specimen was then undergone a histological process using the hematoxylin and eosin (H&E) stain. The histological image captured by microscope (Eclipse TS100 with digital camera DXM 1200C, Nikon Instrucments Inc., Tokyo, Japan) is shown in Fig. 7(b) demonstrating detailed identification of intima, media, and adventitia. The IVUS image correlated well with the histological photo.

## CONCLUSIONS

A highly open system for IVUS imaging was developed and evaluated in this paper. It achieved reconfigurable hardware circuitry, programmable processing algorithms, flexible imaging control, and raw RF data acquisition for various IVUS applications. We demonstrate that the open structure may enable IVUS to combine with other techniques to facilitate multi-modality imaging and comprehensive diagnosis of cardiovascular diseases. In addition, a miniaturized ultrasound catheter probe was designed and fabricated with PMN-PT single crystal to achieve high sensitivity and broad bandwidth. Such an open system can be a valuable platform to combine different capable approaches to form a multi-modality technology to improve diagnosis accuracy and treatment effectiveness for the cardiovascular disease.

## ACKNOWLEDGEMENTS

The authors would like to thank Linda Pet Chui Kwan for the help of histology, and the Hong Kong Research Grant Council (RGC) General Research Fund (GRF) (PolyU 5301/09E), the Hong Kong Polytechnic University (A-PJ84), the Hong Kong Innovative Technology Council (Project No.: ITS/044/09 FP), and the Centre for Smart Materials of the Hong Kong Polytechnic University for the financial supports.

## REFERENCES

[1] P. Libby, “The forgotten majority: unfinished business in cardiovascular risk reduction,” J Am Coll Cardiol., vol. 46, no. 7, pp. 1225-1228, 200.

[2] R. Ross, “Atherosclerosis - An inflammatory disease,” N Engl J Med., vol. 340, no. 2, pp. 115-126, 1999.

[3] R. Virmani, F. D. Kolodgie, A. P. Burke, A. Farb, and S. M. Schwartz, “Lessons from sudden coronary death: a comprehensive morphological classification scheme for atherosclerotic lesions,” Arterioscler Thromb Vasc Biol., vol. 20, no. 5, pp. 1262-1275, 2000.

[4] G. Pasterkamp, and E. Falk, “Atherosclerotic Plaque Rupture: an Overview, Atherosclerotic Plaque Rupture,” J Clin Basic Cardiol., vol. 3, no. 2, pp. 81-86, 2000.

[5] G. Pasterkamp, E. Falk, H. Woutman, and C. Borst, “Techniques characterizing the coronary atherosclerotic plaque: Influence on clinical decision making,” J. Am. Coll. Cardiol., vol. 36, no. 1, pp. 13-21, 2000.

[6] D. H. Blankenhorn, S. P. Azen, M. Kramsch, et al., “Coronary angiographic changes with lovastatin therapy: The monitored atherosclerosis regression study (MARS),” Ann intern med., vol. 119, no. 10, pp. 969-976, 1993.

[7] J. J. Kastelein, and E. de Groot. "Ultrasound imaging techniques for the evaluation of cardiovascular therapies," Eur Heart J., vol. 29, no. 7, pp. 849-58, 2008.

[8] S. J. Nicholls, I. Sipahi, P. Schoenhagen, T. Crowe, E. M. Tuzcu, and S. E. Nissen, "Application of intravascular ultrasound in anti-atherosclerotic drug development," Nat Rev Drug Discov., vol. 5, no.6, pp. 485-492, 2006.

[9] C. L. de Korte, A. F. W. van der Steen, E. I. Cespedes, G. Pasterkamp, S. G. Carlier, F. Mastik, A. H. Schoneveld, P. W. Serruys, and N. Bom, "Characterization of plaque components and vulnerability with intravascular ultrasound elastography," Phys. Med. Biol., vol. 45, no. 6, pp. 1465-1475, 2000.

[10] M. Hartmann, J. Huisman, D. Bose, L. O. Jensen, P. Schoenhagen, G. S. Mintz, R. Erbel, and C. von Birgelen, "Serial intravascular ultrasound assessment of changes in coronary atherosclerotic plaque dimensions and composition: an update," Eur J Echocardiogr., vol. 12, no. 4, pp. 313-321, 2011.

[11] P. A. Lemos, F. Saia, J. M. R. Ligthart, et al., "Coronary restenosis after sirolimus-eluting stent implantation: morphological description and mechanistic analysis from a consecutive series of cases," Circulation, vol. 108. No. 3, pp. 257-260, 2003.

[12] J. A. Kobashigawa1, J. M. Tobis, R. M. Mentzer, H. A. Valantine, R. C. Bourge, M. R. Mehra, F. W. Smart, L. W. Miller, Koji Tanaka, Haiyan Li, D. W. Gjertson, and R. D. Gordon, "Mycophenolate mofetil reduces intimal thickness by intravascular ultrasound after heart transplant: reanalysis of the multicenter trial," Am J Transplant. , vol. 6, no. 5p1, pp. 993-997, 2006.

[13] J. A. Kobashigawa, J. M. Tobis, R. C. Starling, E. M. Tuzcu, A. L. Smith, H. A. Valantine, A. C. Yeung, M. R. Mehra, H. Anzai, B. T. Oeser, K. H. Abeywickrama, J. Murphy, and N. Cretin, "Multicenter intravascular ultrasound validation study among heart transplant recipients: outcomes after five years," J Am Coll of Cardiol., vol. 45, no. 9, pp. 1532-1537, 2005.

[14] G. S. Mintz, and A. Maehara, "Serial intravascular ultrasound assessment of atherosclerosis progression and regression: state-of-the-art and limitations," Circ J. vol. 73, no. 9, pp.1557-1560, 2009.

[15] F. Alfonso, and L. Hernando, "Intravascular ultrasound tissue characterization. I like the rainbow but…what's behind the colours?" Eur Heart J., vol. 29, no. 14, pp. 1701-1703, 2008.

[16] S. Waxman, S. R. Dixon, P. L'Allier, et al., "In vivo validation of a catheter-based near-infrared spectroscopy system for detection of lipid core coronary plaques: initial results of the SPECTACL Study," JACC Cardiovasc Imaging, vol. 2, no. 7, pp. 858-868, 2009.

[17] C. J. Schultz, P. W. Serruys, M. van der Ent, et al., "First-in-man clinical use of combined near-infrared spectroscopy and intravascular ultrasound: a potential key to predict distal embolization and no reflow?" J Am Coll Cardiol., vol. 56, no.4, pp. 314, 2010.

[18] I. K. Jang, B. E. Bouma, D. H. Kang, et al., "Visualization of coronary atherosclerotic plaques in patients using optical coherence tomography: comparison with intravascular ultrasound," J Am Coll Cardiol., vol. 39, no. 4, pp. 604-609, 2002.

[19] Y. Sun, J. Park, D. N. Stephens, J. A. Jo, L. Sun, J. M. Cannata, R. M. G. Saroufeem, K. K. Shung, and L. Marcu, "Development of a dual-modal tissue diagnostic system combining time-resolved fluorescence spectroscopy and ultrasonic backscatter microscopy", Rev Sci Instrum., vol. 80, no. 6, 2009.

[20] S. Sethuraman, S. R. Aglyamov, J. H. Amirian, R. W. Smalling, and S. Y. Emelianov, "Intravascular photoacoustic imaging using an IVUS imaging catheter," IEEE Trans. Ultrason., Ferroelectr., Freq. Control, vol. 54, no. 5, pp. 978-986, 2007.

[21] T. Sawada, J. Shite, H. M. Garcia-Garcia, et al., "Feasibility of combined use of intravascular ultrasound radiofrequency data analysis and optical coherence tomography for detecting thin-cap fibroatheroma," Eur. Heart J. vol. 29, no. 9, pp. 1136-1146, 2008.

[22] X. Li, J. Yin, C. Hu, Q. Zhou, K. K. Shung, and Z. Chen, "High-resolution coregistered intravascular imaging with integrated ultrasound and optical coherence tomography probe," Appl Phys Lett., vol. 97, no. 13, 2010.

[23] H. C. Yang, J. Yin, C. Hu, J. Cannata, Q. Zhou, J. Zhang, Z. Chen, and K. K. Shung, "A dual-modality probe utilizing intravascular ultrasound and optical coherence tomography for intravascular imaging applications," IEEE Trans. Ultrason. Ferroelectr. Freq. Control, vol. 57, no. 12, pp. 2839-2843, 2010.

[24] X. Xu, J. T. Yen, and K. K. Shung, "A low-cost bipolar pulse generator for high frequency ultrasound applications," IEEE Trans. Ultrason., Ferroelectr., Freq. Control, vol. 54, no. 2, pp. 443-447, 2007.

[25] L. Sun, X. Xu, W. D. Richard, C. Feng, J. A. Johnson and K. K. Shung, "A high-frame rate duplex ultrasound biomicroscopy for small animal imaging In vivo," IEEE Trans. Biomed. Eng., vol. 55, No. 8, pp. 2039-2049, 2008.

[26] L. Sun, C. Lien, X. Xu and K. K. Shung, "In vivo cardiac imaging of adult zebrafish using high frequency ultrasound (45-75 MHz)," Ultrasound Med. Biol., vol. 34, No. 1, pp. 31-39, 2008.

[27] Q. Zhou, X. Xu, E. J. Gottlieb, L. Sun, J. M. Cannata, H. Ameri, M. S. Humayun, P. Han, and K. K. Shung, "PMN-PT single crystal, high-frequency ultrasonic needle transducers for pulsed-wave Doppler application," IEEE Trans. Ultrason. Ferroelectr. Freq. Control, vol. 54, no. 3, pp. 668-675, 2007.

[28] E. L. Madsen, G. R. Frank, M. M. McCormick, M. E. Deaner, and T. A. Stiles, "Anechoic sphere phantoms for estimating 3-D resolution of very-high-frequency ultrasound scanners," IEEE Trans. Ultrason. Ferroelectr. Freq. Control, vol. 57, no. 10, pp. 2284-2292, 2010.